# Acquisition of ionic copper by a bacterial outer membrane protein

Satya Prathyusha Bhamidimarri[1], Tessa R. Young[2], Muralidharan Shanmugam[3], Sandra Soderholm[4], Bastien Belzunces[5], Arnaud Baslé[1], Chris Skylaris[5], Dirk Bumann[4], Syma Khalid[5], Bert van den Berg[1#]

[1]Biosciences Institute, The Medical School, Newcastle University, Newcastle upon Tyne NE2 4HH, UK

[2]Department of Biosciences, Durham University, DH1 3LE Durham, UK.

[3]Manchester Institute of Biotechnology, University of Manchester, 131 Princess Street, Manchester M1 7DN, UK

[4] Focal Area Infection Biology, University of Basel, CH-4056 Basel, Switzerland

[5]School of Chemistry, University of Southampton, Southampton SO17 1BJ, UK

[#] Corresponding author: bert.van-den-berg@ncl.ac.uk

## Abstract

Copper, while toxic in excess, is an essential micronutrient in all kingdoms of life due to its essential role in the structure and function of many proteins. Proteins mediating ionic copper import are known in eukaryotes, but have not yet been described in prokaryotes. Here we show that *Pseudomonas aeruginosa* OprC is a TonB-dependent transporter that mediates acquisition of ionic copper. Crystal structures of wild type and mutant OprC variants with silver and copper, as well as ICP-MS and electron paramagnetic resonance (EPR), suggest that binding of Cu(I) occurs via a surface-exposed methionine track leading towards an unprecedented CxxxM-HxM metal binding site that binds Cu(I) directly and can facilitate reduction of Cu(II) via the cysteine thiol. Together with quantitative proteomics and growth assays, our data identify OprC as an abundant component of bacterial copper biology that enables copper acquisition and potentially copper storage under a wide range of environmental conditions.

## Introduction

Metals fulfil cellular functions that cannot be met by organic molecules and are indispensable for the biochemistry of life in all organisms. Copper is the third-most abundant transition metal in biological systems after iron and zinc. It has key roles as structural component of proteins or catalytic cofactor for enzymes[1], most notably associated with the biology of oxygen and in electron transfer. On the other hand, an excess of copper can be deleterious due to its ability to catalyse production of hydroxyl radicals[2, 3]. Excessive copper may also disrupt protein structure by interaction with the polypeptide backbone, or via replacement of native metal cofactors from proteins, thus abolishing enzymatic activities via mismetallation[4, 5]. Thus, cellular copper levels and availability must be tightly controlled. Bacterial copper homeostasis systems are well characterised[6]. Specific protein machineries are involved in fine-tuning the balance of intracellular copper trafficking, storage and efflux according to cellular requirement, in such a way that copper is always bound inside the cell. This control is executed by periplasmic and cytosolic metalloregulators, which activate transcription of periplasmic multi-copper oxidases, metallochaperones, copper-sequestering proteins[7, 8] and transporters[9-11]. To date, relatively few families of integral membrane proteins have been validated as copper transporters, and these have different structures and transport mechanisms[12]. The $P_{1B}$-type ATPases such as CopA are responsible for Cu(I) efflux from the cytosol via several metal binding domains, using energy released from ATP hydrolysis[13-15]. A second class of copper export proteins are RND-type tripartite pumps such as CusABC, which efflux Cu(I) by utilising the proton-motive force[16-18]. Relatively few copper influx proteins have been identified. The inner membrane copper importer CcoA is a major facilitator superfamily (MFS)-type

transporter involved in fine-tuning the trafficking of copper into the cytosol and required for cytochrome c oxidase maturation[19, 20]. The Ctr family of copper transporters is responsible for Cu(I) translocation into the cell without requiring external sources of energy[21]. However, Ctr homologs are found only in eukaryotes, and the molecular mechanisms by which copper ions enter bacteria is still a matter of debate. The exception is copper import via metallophores like methanobactin, a small Cu-chelating molecule that is secreted by methanotropic bacteria and most likely taken up via TonB-dependent transporters, analogous to iron-siderophores[22].

*Pseudomonas aeruginosa* is a versatile and ubiquitous Gram-negative bacterium that promotes infections in several hosts and multiple sites. It is a notorious opportunistic pathogen in humans, and is mainly responsible for the development of chronic lung infection in cystic fibrosis patients[23, 24]. *P. aeruginosa* has a number of TonB-dependent transporters (TBDTs) in the outer membrane (OM) dedicated to the acquisition of different iron-siderophore complexes such as pyochelin and pyoverdin[25]. In addition, *P. aeruginosa* contains another TBDT, termed OprC (*PA3790*), whose function has remained enigmatic. Nakae *et al*. suggested that OprC binds Cu(II) with micromolar affinities[26]. Transcription of OprC was recently found to be repressed in the presence of Cu(II) in the external medium under aerobic conditions[27], suggesting a role for OprC in copper acquisition. Very recently, the blue copper protein azurin was reported to be secreted by a *P. aeruginosa* Type VI secretion system and to interact with OprC, suggesting a role of the latter in Cu(II) uptake[27].

To clarify the role of OprC in copper biology, we have determined X-ray crystal structures of wild type and mutant OprC proteins in the absence and presence of copper and silver, and characterised metal binding via ICP-MS, EPR and quantum chemistry calculations. OprC indeed has the typical structure of a TBDT, and differences between the Cu-loaded and Cu-free protein demonstrate changes in tertiary structure that likely lead to TonB interaction. Strikingly, metal binding experiments show that while OprC can bind to both Cu (I) and Cu (II) *in vitro*, only Cu (I) is present at the principal CxxxM-HxM metal binding site, suggesting that Cu(I) is the imported redox state and that reduction of Cu(II) may be mediated by OprC.

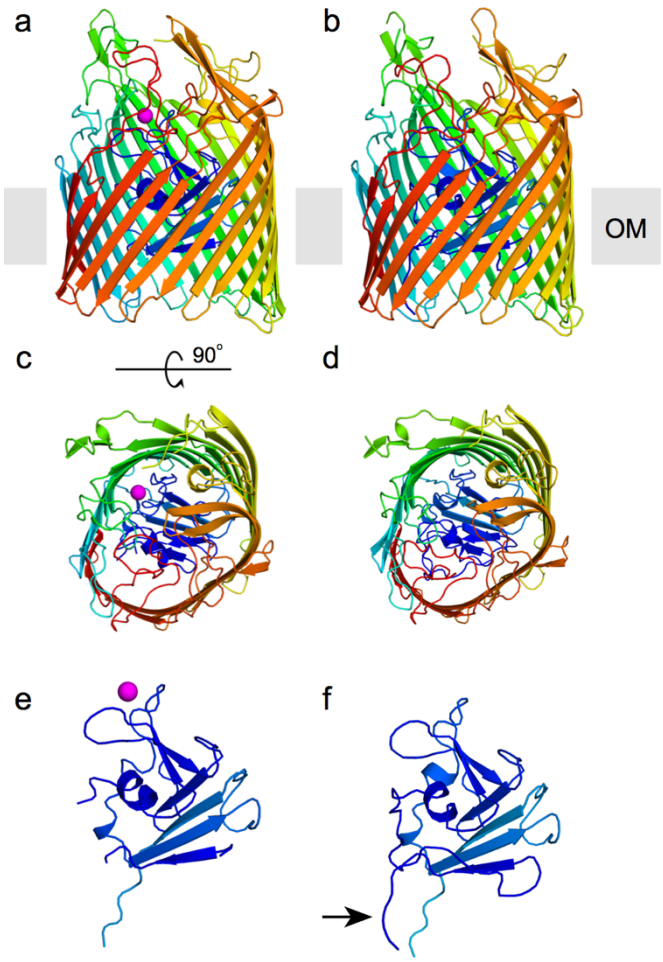


**Figure 1. OprC is a TonB-dependent transporter.** Cartoon representation of (**a,c**) Cu-loaded OprC and (**b,d**) Cu-free OprC ($OprC_{AA}$). The N-terminal plug domain is shown separately for both forms (**e,f**). Structures are shown in rainbow from N-terminus (blue) to C-terminus (red); copper is represented as a magenta sphere. The arrow in (**f**) highlights the visibility of the Ton box in apo-OprC.

## Results

### OprC is a TonB-dependent transporter that binds ionic copper

The structure of OprC crystallised under aerobic conditions in the presence of 2 mM $CuCl_2$ was solved using single wavelength anomalous dispersion (SAD), using data to 2.0 Å resolution (Methods; Supplementary Table 1; Supplementary Fig. 1). As indicated by the successful structure solution, OprC contains bound copper and shows the typical fold of a TBDT, with a large 22-stranded β-barrel occluded by an N-terminal ~15 kDa plug domain (Fig. 1). The copper binding site comprises residues Cys143 and Met147 in the plug domain and His323 and Met325 in the barrel wall. The CxxxM-HxM configuration, which coordinates the copper in a tetrahedral manner (Fig. 2a, b), is highly unusual and has, to our knowledge, not been observed before in copper homeostasis proteins. The most similar site is present for one of the copper ions of the valence-delocalised $Cu_A$ dimer in cytochrome c oxidase, where the

121 copper ion is coordinated by 2Cys+1Met+1His[28, 29]. The other relevant sites are class I Type I
122 copper proteins like pseudoazurin and plastocyanin, where copper is coordinated by
123 2His+1Cys+1Met[30]. Interestingly, and unlike class I Type I copper proteins, concentrated
124 solutions and OprC crystals are colourless in the presence of Cu(II). Another notable feature
125 of the OprC structure becomes apparent when analysing the positions of the methionine
126 residues. As shown in Fig. 2d, out of the 15 visible methionines in OprC, 10 are organised in
127 such a way that they form a distinct "track" leading from the extracellular surface towards the
128 copper binding site. An additional two methionines are not visible due to loop disorder, but
129 given their positions (Met448, Met558) they will be a part of the methionine track. We propose
130 that the methionine track serves to bind copper with low affinity and may guide the metal
131 towards the principal binding site. It should be noted that the anomalous difference maps of
132 OprC crystallised in the presence of Cu(II) do not show any evidence for weaker, secondary
133 copper sites (Supplementary Fig. 1).
134

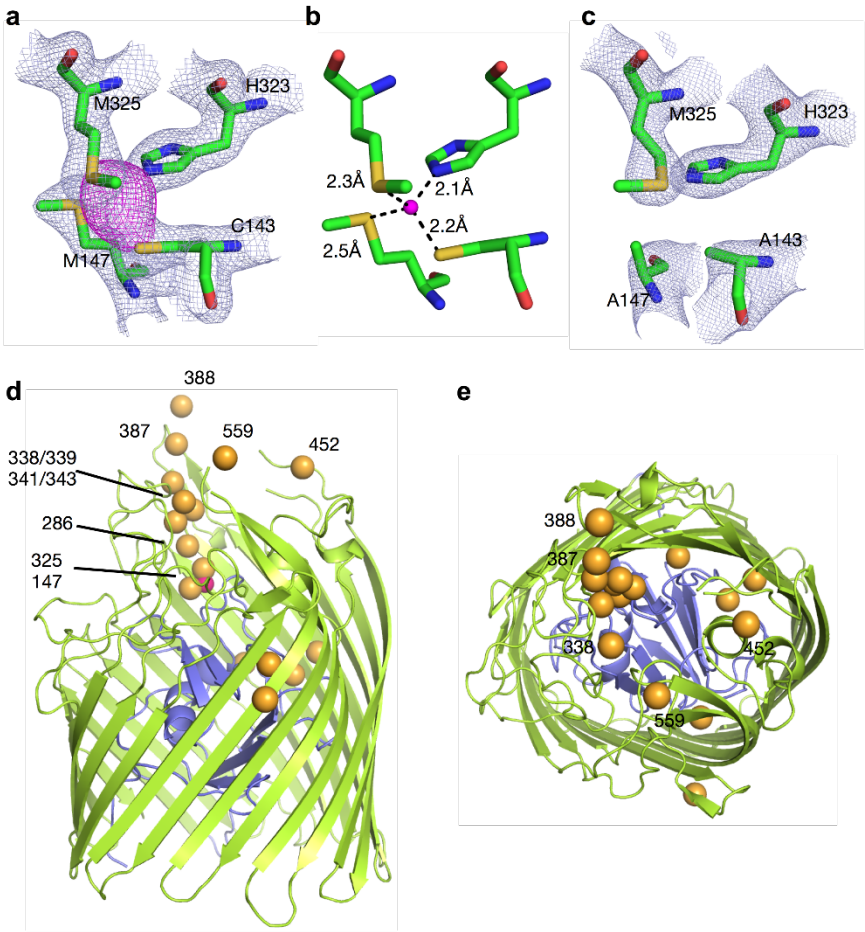


135
136 **Figure 2. OprC has an unusual CxxxM-HxM binding site and a methionine binding track.**
137 **a,** Stick models of copper-coordinating residues Cys143, Met147, Met325 and His323.
138 Electron density in gray mesh (2Fo-Fc map contoured at 2.0σ, carve = 2.0) is shown for the
139 binding site residues C/M-H/M and the copper atom (anomalous difference map shown in

magenta, contoured at 3.0σ, carve = 2.25). **b,** Distances between coordinating residues and metal show that copper is coordinated via 1 thiolate (from Cys), two thioethers (from Met), and one imidazole nitrogen from His. **c,** Mutation of binding site residues Cys143 and Met147 to alanines abolishes copper binding (2Fo-Fc map contoured at 2.0σ, carve = 2.0). **d,e,** OM plane **(d)** and extracellular views **(e)** showing the thioether atoms of all methionine residues present in OprC as yellow spheres.

**Copper binding by OprC is highly specific and near-irreversible.**

Following structure determination of copper-bound OprC, several attempts were made to produce a structure of copper-free OprC. First, the protein was purified and crystallised without added copper; this gave a structure that was identical to the one already obtained and contained bound copper that presumably originated from the LB medium. As expression in rich media always yielded OprC with ~1 equivalent copper as judged by ICP-MS, various attempts to lower the copper content were made. Removal of bound copper from purified protein with combinations of denaturants (up to 4.0 M urea) and EDTA were not successful. Expression in chelex-treated minimal medium reduced, in the best cases, the metal content of the wild type to ~45 % equivalency as assessed by ICP-MS (Fig. 3a). Subsequent incubation of OprC for 30 min in the presence of either 3 or 10 equivalents Cu(II) followed by size exclusion chromatography (SEC) and ICP-MS analysis of the peak fractions leads to co-elution and occupancy of 1 equivalent copper (Fig. 3a). However, co-incubation with 1 mM EDTA (~100-fold excess) does not result in copper loading, suggesting that EDTA effectively withholds copper from OprC (Supplementary Fig. 2). As-purified OprC does not contain zinc, a common contaminant in metal-binding proteins, indicating that OprC is highly specific. Indeed, incubation of purified OprC in the presence of 3 or 10 equivalents Zn does not result in zinc co-elution (Supplementary Fig. 2). To obtain copper-free OprC, we constructed a variant in which the binding site residues Cys143 and Met147 were both mutated to alanines, generating copper-free protein ($OprC_{AA}$) after purification from rich media (Fig. 3a; AA). Even after equilibration of $OprC_{AA}$ for 30 min with 3 or 10 equivalents Cu(II) no co-elution with metal is observed (Fig. 3a), indicating that high-affinity copper binding is completely abolished. It should be noted that $OprC_{AA}$ contains a His-tag, demonstrating that Cu(II) does not bind to the His-tag of OprC with an affinity high enough to survive SEC, possibly due to the presence of 0.5 mM EDTA in the SEC buffer.

The fact that it is not possible to obtain copper-free wild type protein, even after taking extensive precautions, suggests that copper binds to OprC with very high affinity. To explore this further, we performed a copper extraction assay with a large excess of bathocuproinedisulfonic acid (BCS) under reducing conditions (Methods). BCS is a high-affinity Cu(I) chelator ($\log\beta_2$ 20.8) and forms a 2:1 complex with Cu(I), namely $[Cu(BCS)_2]^{-3}$, with a molar extinction coefficient of 13,300 $cm^{-1}$ $M^{-1}$ at 483nm, enabling quantitation of Cu(I).

179 For copper-loaded $OprC_{WT}$, only 20% copper was removed after 24 hrs at room temperature,
180 and the temperature had to be increased to 60 °C to obtain near-quantitative extraction of
181 copper (~90% after 24 hours) (Fig. 3b). For reasons that are unclear, the orange-coloured
182 $[Cu(BCS)_2]^{-3}$ complex was hard to separate from OprC, and BCS-treated OprC did not bind
183 copper anymore, suggesting an irreversible change in the protein due to the harsh incubation
184 conditions. These results demonstrate that copper is kinetically trapped inside OprC and is,
185 for all intents and purposes, irreversibly bound. This is compatible with the consensus
186 transport mechanism of TBDTs, in which the interaction with TonB is thought to result in the
187 disruption of the binding site and subsequent release of the substrate[31].
188

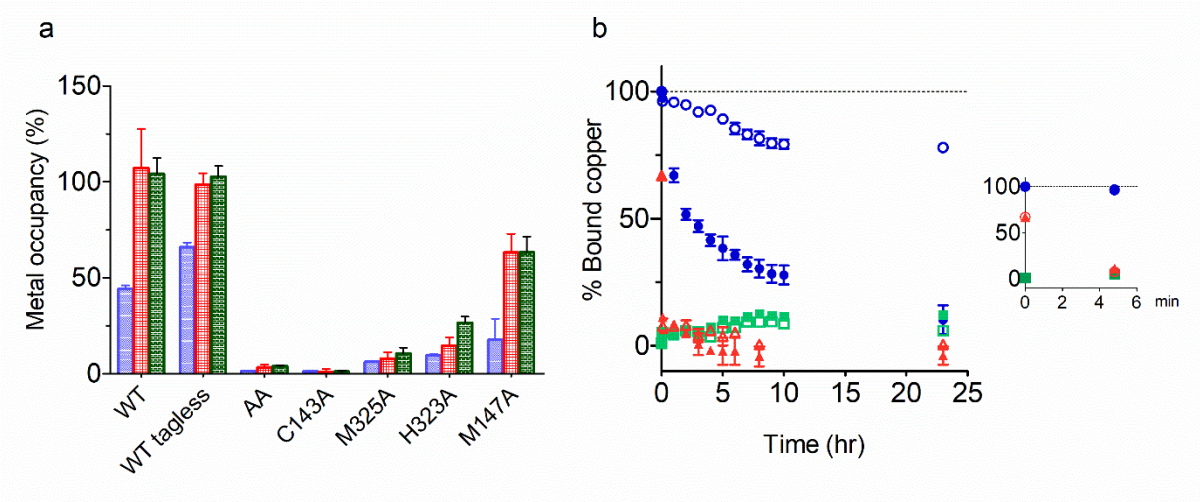


189

190 **Figure 3. OprC binds to up 1 equivalent copper near-irreversibly. a,** Copper content of
191 wild type OprC and binding site mutant proteins before (blue) and after aerobic incubation with
192 either 3 (red) or 10 equivalents Cu(II) (green) for 30 min followed by analytical SEC and quan-
193 titation of the copper content of the OprC peak by ICP-MS. "As purified" metal contents were
194 obtained from MM-grown *E. coli* cells for WT OprC and from LB-grown cells for all mutant
195 proteins. All proteins except where stated contain a C-terminal hexa-histidine tag. The in-
196 crease in copper content in "as purified" tagless WT protein is most likely due to the use of a
197 second IMAC column after tag cleavage. Reported values are averages ± s.d. (n = 3) **b,** Cop-
198 per is kinetically trapped in OprC. Time course of copper extraction experiments showing %
199 bound copper for OprC WT (blue), $OprC_{AA}$ (green) and OprC M147A (red), at room tempera-
200 ture (open symbols) and 60 °C (filled symbols). The inset shows % bound copper in the first
201 few minutes after starting the experiment. $OprC_{AA}$ served as a control. Reported values are
202 averages ± s.d. (n = 3)
203

204 **Conformational changes upon copper binding.**

205 The $OprC_{AA}$ structure was solved by molecular replacement using Cu-bound OprC as the
206 search model (Fig.1b, d, f; Fig. 2c). The binding site residues of both structures occupy very
207 similar positions, indicating that the introduced mutations abolish copper binding without
208 generating gross changes in the binding site. Superposition of the structures (Figs. 4 a,b)
209 shows that for the remainder of the transporter, structural changes upon copper binding are
210 confined to the vicinity of the copper binding site, with parts far removed virtually unchanged

211 (overall Cα r.m.s.d ~ 1.0 Å). The largest change is observed for loop L11, which undergoes an
212 inward-directed motion of ~ 8.0 Å upon copper binding (Figs. 4 d,e and Supplementary Fig.
213 3). A similar inward-directed but smaller change occurs for loop L8. Some loop tips (*e.g.* L4,
214 L5, L6) in $OprC_{AA}$ lack electron density for a limited number of residues, suggesting increased
215 mobility. However, given that the proteins were crystallised in different space groups (OprC,
216 $C222_1$; $OprC_{AA}$ $P22_12_1$), such differences could also be the result of different crystal packing.
217 Overall, the conformational changes of the loops decrease the accessibility of the copper
218 binding site. However, the main reason why the bound copper is inaccessible to solvent is
219 because the binding site residues Met147 and Met325, together with Asn145, effectively form
220 a lid on the copper ion. In the double mutant, copper becomes solvent accessible due to the
221 absence of the Met147 side chain (Fig. 4d and Supplementary Fig. 3).
222

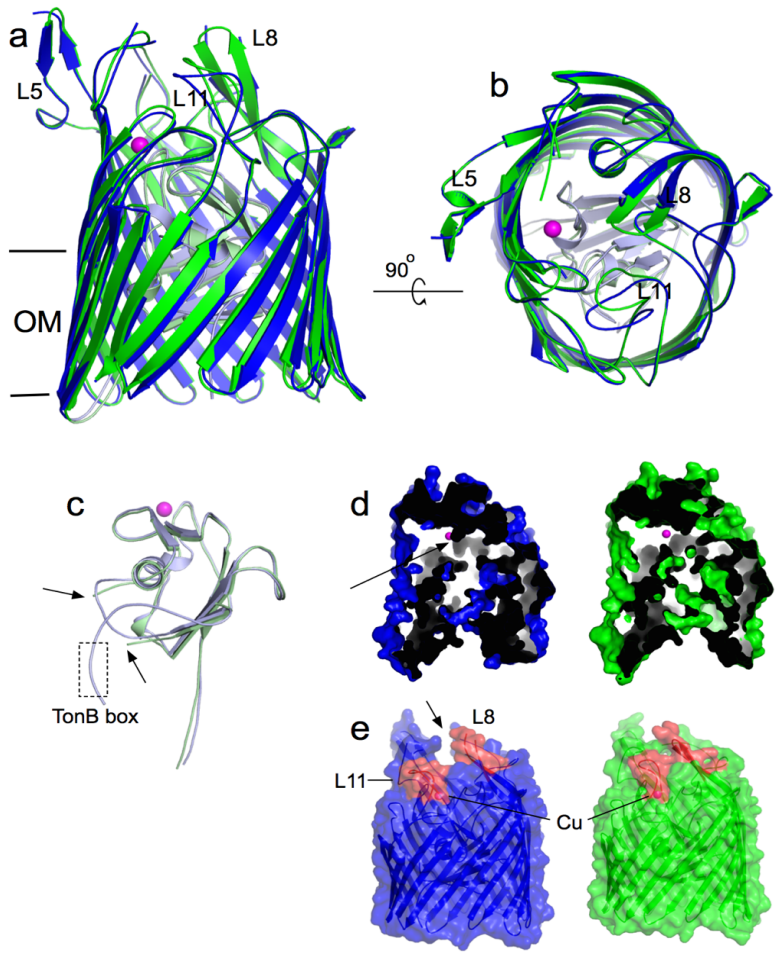


223

224 **Figure 4. OprC structural changes upon copper binding. a,b** Cartoon superposition from
225 the OM plane (**a**) and extracellular environment (**b**) of OprC (coloured green) and $OprC_{AA}$
226 (blue), indicating locations of loops L5, L8 and L11; copper is represented as a magenta
227 sphere. The plug domains of OprC and $OprC_{AA}$ are coloured light green and light blue,
228 respectively. **c,** N-terminal plug domains indicating the location of the TonB box, which is
229 invisible in Cu-bound OprC. Arrows indicate the missing density for Glu88-Pro94 in OprC. **d,**
230 Surface slab representations from the OM plane, showing the presence of a solvent pocket in

231 $OprC_{AA}$ that is generated by the absence of Met147 (arrow). For orientation purposes, the
232 location of OprC-bound copper is shown in both structures. **e,** Side surface views showing the
233 conformational changes of L8 and L11 (coloured red) as a result of copper binding. As in **(d)**,
234 the bound copper of OprC is shown in both proteins.
235
236 The current consensus mechanism for TonB-dependent transport postulates that ligand
237 binding on the extracellular side generates conformational changes that are propagated to the
238 periplasmic side of the plug and increase the periplasmic accessibility of the Ton box for
239 subsequent interaction with TonB[32]. In $OprC_{AA}$, N-terminal density is visible up to Leu66 (*i.e.*,
240 the first 10 residues of the mature protein are disordered) including the Ton box
241 ($^{68}$PSVVTGV$^{75}$), which is tucked away against the plug domain and the barrel wall. In Cu-
242 bound OprC, the density between Glu88 and Pro94 is hard to interpret and, more importantly,
243 no density is observed before Pro79, including the Ton box (Figs. 1e, f and 4c). Thus, the
244 structures of OprC in the absence and presence of ligand conform to the consensus transport
245 mechanism, in the sense that the TonB box is accessible for potential interaction with
246 periplasmic TonB only in the substrate-loaded protein. This would prevent non-productive
247 interactions with transporters that do not have substrate bound[32].
248
249 **The OprC methionine track binds Cu(I) but not Cu(II).**
250 Which redox state of the copper ion is present in OprC? Since it is challenging to maintain
251 copper in its +1 state during crystallisation, we used silver ($Ag^+$) as a proxy for Cu(I) and
252 determined the co-crystal structure of WT OprC in the presence of 2 mM $AgNO_3$ (Methods).
253 Data was collected at 8000 eV, at which energy the anomalous signal of copper is very small
254 (0.6 $e^-$, compared to 4.2 $e^-$ for Ag). Strikingly, and in sharp contrast to copper (Supplementary
255 Fig. 1), the anomalous map of OprC WT crystallised in the presence of silver shows not one
256 but three anomalous peaks. The first, strong peak (Ag1; 23$\sigma$) is located at the same site as in
257 OprC crystallised with copper, and is coordinated by the same residues (Cys143, Met147,
258 His323 and Met325; Fig. 5). The other two sites have lower occupancy (Ag2, ~10$\sigma$ and Ag3,
259 ~10$\sigma$) and are each coordinated by two methionines in the methionine track (Met286 and
260 Met339 for Ag2; Met341 and Met343 for Ag3). This structure therefore suggests that the
261 methionine track provides several low-affinity binding sites for Cu(I) ions, and that the high
262 affinity CxxxM-HxM site binds Cu(I).
263
264 To obtain more information on the individual residue contribution to copper binding, we next
265 generated the complete set of single alanine mutants of the principal binding site residues
266 (C143A, M147A, H323A and M325A), and determined copper binding via analytical SEC and
267 ICP-MS. For all single mutants, the copper content after purification from LB was below 10%,
268 except for M147A (~20 %) (Fig. 3a). Upon incubation with 3 or 10 equivalents Cu(II), various

occupancies were obtained. C143A has no bound copper even after incubation with 10 equivalents Cu (II), suggesting this residue has a crucial role. H323A (~30%) and in particular

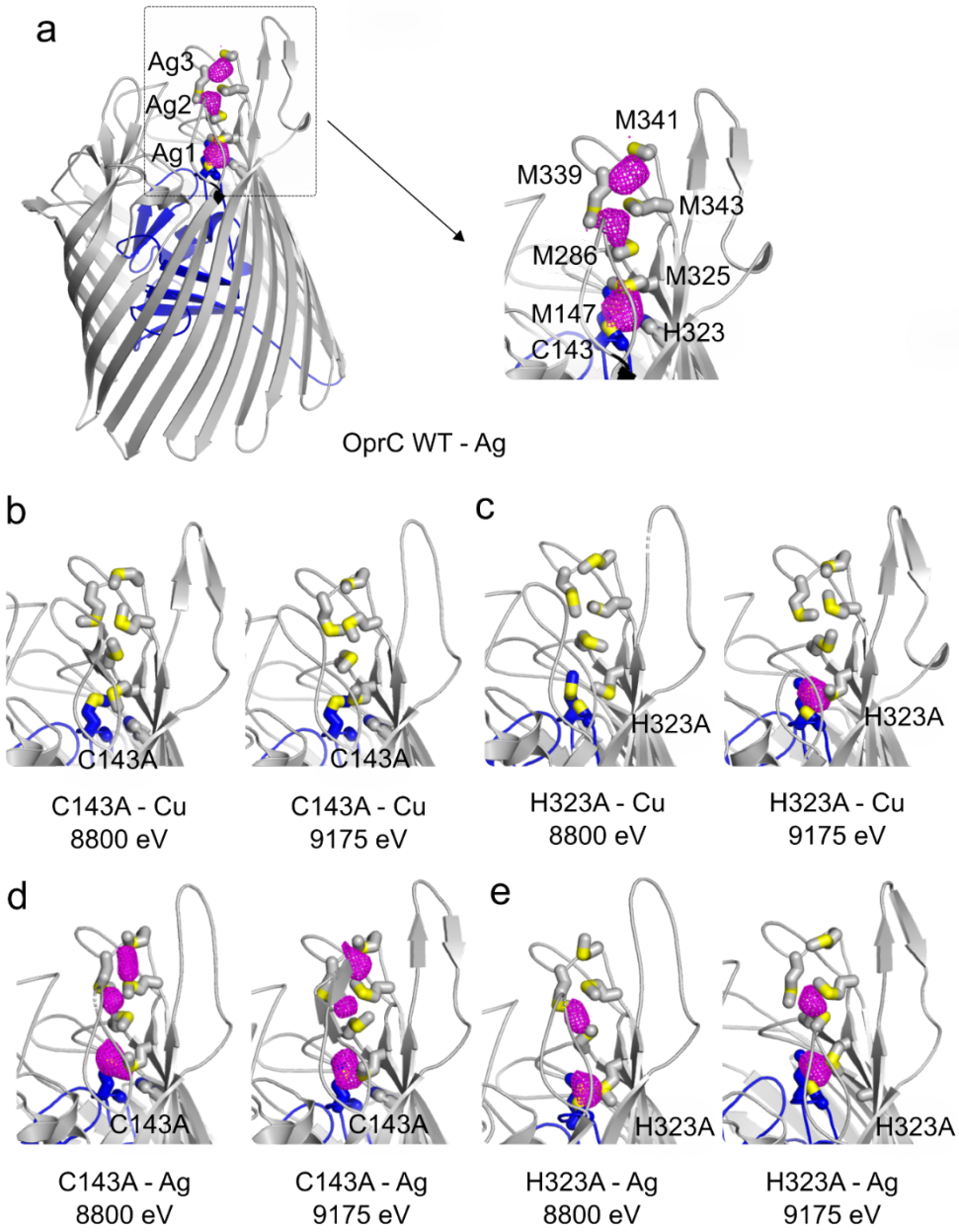


**Figure 5 OprC binds Cu(I). a-e**, Anomalous difference maps of (**a**) OprC wild type, (**b,d**) C143A and (**c,e**) H323A variants crystallised in the presence of (**a,d,e**) Ag or (**b,c**) Cu(II), and collected at different energies. The inset to (**a**) shows a close-up of the anomalous difference peaks (magenta) near the principal binding site in wild type OprC, with binding residues labelled and represented as stick models. Sulphurs are coloured yellow. For clarity, the metal used in co-crystallisation and the energy used for data collection are shown underneath each panel. The OprC plug domain is coloured blue.

318 M147A (~60%) have relatively high occupancies after copper incubation and SEC, indicating
319 that these residues contribute less towards binding. Of the four ligands, the M147 thioether is
320 the furthest away from the copper in the crystal structure (Fig. 2b), which may explain why it
321 contributes the least to ligand binding. Interestingly, removal of bound copper is much faster
322 in the M147A mutant compared to $OprC_{WT}$ (Fig. 3b), suggesting that solvent exclusion by the
323 M147 side chain (Fig. 4d) is the main reason why copper is kinetically trapped in the wild type
324 protein.
325
326 **Cu(II) is reduced by the principal binding site cysteine.**
327 The fact that wild type OprC and most single alanine mutants can be loaded via Cu(II)
328 incubation (Fig. 3a) suggests that Cu(II) is also a substrate for the transporter. However, the
329 complete lack of copper in the C143A mutant is intriguing (Fig. 3a) and could be explained in
330 two ways. If one assumes that OprC can bind Cu(II), removal of the cysteine could lead to
331 much lower affinity for Cu(II), so that after SEC nothing remains bound. Alternatively, if OprC
332 only binds Cu(I), the lack of the cysteine could prevent reduction of added Cu(II). To distinguish
333 between these two possibilities, we determined the crystal structures of the OprC C143A and
334 H323A mutants in the presence of either Cu(II) or Ag(I). For each crystal, two datasets were
335 collected at different energies. The first energy (8800 eV) is below the copper K-edge (8979
336 eV), while the second one is above the edge (9175 eV), giving small and large anomalous
337 signals for copper (0.5 and 3.7 $e^-$ respectively). For silver, substantial anomalous signal is
338 present at both energies (~3.6 $e^-$). Thus, bound copper is expected to give a strong anomalous
339 peak only at 9175 eV, while silver will give comparable peaks at both energies. For C143A co-
340 crystallised with copper, no anomalous peaks are visible at both energies (Fig. 5b), showing
341 a lack of bound copper. Crucially, in the presence of silver, the same three anomalous peaks
342 are visible as for wild type OprC (Figs. 5 a, d), strongly suggesting that the C143A mutant does
343 still bind Cu(I). The H323A mutant, on the other hand, still binds copper supplied as Cu(II),
344 and also binds silver (Figs. 5 c, e). Together, these data therefore suggest that (i) Cys143
345 reduces Cu(II) to Cu(I) and (ii) OprC does not bind Cu(II) specifically. To support the notion
346 that the principal OprC binding site is a reducing environment, we performed quantum
347 chemistry calculations for a 70-atom system consisting of the OprC binding site, containing
348 either Cu(I) or Cu(II) (Methods). The absolute energies show that the system with Cu(I) is 221
349 and 133 kcal/mol more stable compared to Cu(II) for the hydrogenated and dehydrogenated
350 forms of Cys respectively (Supplementary Table 4). Energy Decomposition Analysis (EDA) of
351 the Cu(I) interaction with Cys143, Met147, Met325 and His323, revealed the total interaction
352 energy of the four residues with Cu(I) to be 96 kcal/mol more stable when cysteine is
353 dehydrogenated (oxidised). The metal protein stabilisation interactions are dominated by

354 electrostatic interactions, with polarization and charge-transfer playing only a minor role.
355 Additional details are provided in the Supplementary Information.
356
357 To shed additional light on the redox state of the bound copper, continuous wave EPR (cw-
358 EPR) spectra were recorded on $OprC_{WT}$ and single/double mutants. As-purified OprC WT con-
359 taining 0.6 equivalents copper was EPR silent (Supplementary Fig. 4; WT-1), confirming the
360 bound species is Cu(I). All other analysed variants were EPR silent as well. Subsequently,
361 proteins were incubated with 0.25 equivalents of $CuSO_4$ and EPR spectra were recorded. The
362 EPR spectra of all the OprC variants showed the appearance of the typical EPR signals as-
363 sociated with a Type(II) copper centre. These EPR signals are significantly different from the
364 standard $CuSO_4$, Cu(II) EPR signals, as inferred from the visual inspection and also from the
365 spectral simulations. The EPR spectra of the OprC variants show nicely resolved $^{63,65}$Cu(II)
366 hyperfine coupling along the parallel region, due to the interaction of an unpaired electron spin
367 ($S$= ½) of Cu(II) with the nuclear spin of ($I$ = 3/2*) of* $^{63,65}$Cu nuclei, as indicated by the magenta
368 goal-post in Supplementary Fig. 4. The intense EPR signal observed at ~3300 G shows super-
369 hyperfine splittings for the $OprC_{AA}$ double mutant and OprC-M147A, arising plausibly from
370 $^{1}$H/$^{14}$N nuclei in close proximity of the Cu(II) ion. The intensities of the EPR signals increased
371 upon addition of further Cu(II) equivalents (Supplementary Fig. 4 and Supplementary Table
372 5). The additional Cu(II) loading caused changes in EPR line widths, which results in broad-
373 ening and/or disappearance of the super-hyperfine splittings for OprC M147A. The analysis of
374 the EPR spectra of $OprC_{WT}$ and OprC-M147A shows the presence of two type(II) Cu(II) EPR
375 active species ($S$ = ½ species), which are not clearly visible by the naked eye in the case of
376 the M147A variant. By contrast, $OprC_{AA}$ and M147H yielded EPR signals arising from single
377 contributing EPR active species. The spectra suggest that Cu(II) does bind to OprC, but not
378 at the principal binding site, as judged from the facts that (i) the spectra resembled that of a
379 Type II copper center [33 34, 35] and (ii) Cu(II) also binds to $OprC_{AA}$. The EPR spectra were suc-
380 cessfully simulated (Supplementary Fig. 5) using the spin-Hamiltonian parameters provided
381 in Supplementary Table 5. Interestingly, the EPR signals for both wild type OprC and the
382 M147A variant decrease slowly upon prolonged incubation (Supplementary Fig. 4). Collec-
383 tively, the EPR data suggest that Cu(II) binds to OprC at one or more sites distinct from the
384 principal binding site, and, via unknown routes, eventually ends up in the principal binding site,
385 where it is reduced to Cu(I). It is possible, and perhaps even likely, that the Cu(II) binding sites
386 as inferred by EPR are adventitious due to the fact that the protein is present in detergent and
387 has much more surface (*e.g.* the entire periplasmic face) available for binding compared to
388 the physiological situation, in which OprC is embedded in the OM and accepts copper from
389 the extracellular environment. The addition of 1-10 equivalents of hydrogen peroxide oxidant
390 directly to the 'as purified' $OprC_{WT}$ has no significant effect on the electronic structure of the

391 bound Cu(I) ion as reflected by the lack of changes in the observed EPR spectra. This is
392 consistent with the solvent inaccessibility of the principal copper binding site in $OprC_{WT}$.
393
394 To confirm that OprC binds the Cu(II) redox state *in vitro*, M147A and $OprC_{AA}$ samples were
395 analysed by recording intrinsic tryptophan fluorescence upon Cu(II) addition. $OprC_{AA}$ was used
396 as a control for which high-affinity copper binding is abolished. After excitation at 300 nm, an
397 emission peak at 340nm was observed in both variants. Subsequent titrations with Cu(II) so-
398 lution showed very similar reductions in the 340 nm emission peak in both OprC M147A and
399 $OprC_{AA}$ (Supplementary Fig. 6). In both cases, saturation is not reached at 3 equivalents cop-
400 per, suggesting that Cu(II) binds non-specifically to OprC, consistent with the position of this
401 metal at the top of the Irving-Williams series. Indeed, at high concentrations (~0.1 mM), OprC
402 precipitates in the presence of millimolar Cu(II). Since OprC has 15 tryptophan residues it is
403 not possible to define the locations of these binding sites.
404
405 **OprC is abundant in *P. aeruginosa* during infection.**
406 To determine the abundance of OprC in *Pseudomonas aeruginosa* UCBPP-PA14 or
407 *Acinetobacter baumannii* ATCC 19606 in infected lung tissues, we employed a sensitive
408 targeted proteomics approach with parallel reaction monitoring, on a high resolution and
409 accurate mass instrument with absolute quantification using heavy-isotope labeled reference
410 peptides (Methods). The results showed that in both mouse and rat pneumonia models, OprC
411 was present at 1,000 to 10,000 molecules per *P. aeruginosa* cell, making it one of the five
412 most abundant TonB-dependent transporters. As a comparison, the most abundant TonB-
413 dependent transporter, FpvA, had 8,000 to 33,000 molecules per cell. We also assessed OprC
414 abundance in *A. baumannii*, due to the facts that both proteins are highly similar (50%
415 sequence identity, Supplementary Fig. 8) and that both bacteria are important human
416 pathogens with a similar, low-permeability OM. In *A. baumannii*, OprC was less abundant in
417 mouse and rat pneumonia models (40 to 400 molecules per cell), while the most abundant
418 TonB-dependent transporters BfnH and BauA were present at 500 to 3'000 molecules per cell.
419
420 **OprC does not confer copper toxicity in *P. aeruginosa in vitro*.**
421 To demonstrate that OprC imports copper, we initially performed growth experiments in an *E.*
422 *coli ΔcopA* strain that should be more susceptible to copper stress. Cells were grown at vari-
423 ous external Cu(II) concentrations (0-6 mM) while expressing plasmid-based wild type OprC
424 or $OprC_{AA}$. Toxicity was observed in all three strains above 1 mM $CuSO_4$, but no differences
425 were observed between the strains. However, the presence of abundant porins in *E. coli*, to-
426 gether with the high copper concentrations, make porin-mediated copper influx likely, and this
427 would mask any contribution from OprC. In addition, it is also not clear whether *E. coli* TonB

428 couples to *P. aeruginosa* OprC. Given that OprC is highly abundant and is expressed during
429 anaerobiosis[26, 36, 37], we next investigated whether OprC causes *in vitro* copper or silver toxicity
430 in *P. aeruginosa* under anaerobic conditions. In rich media, excessive copper concentrations
431 (mM) are required to cause toxicity, and no differences are observed for PA14 wild type and
432 Δ*oprC* strains (Supplementary Fig. 7), in line with recent data showing that *oprC* is repressed
433 in the presence of mM external copper under aerobic conditions[27]. We next assessed minimal
434 media, in which toxicity was observed at μM concentrations of copper (Fig. 6). However, PA14
435 wild type and Δ*oprC* strains still had similar phenotypes, and only occasionally did we observe
436 better growth for the Δ*oprC* strain over a very narrow range of copper concentrations (Supple-
437 mentary Fig. 7c, d). Silver causes toxicity at 10-fold lower concentrations compared to copper,
438 but again, no clear differences in growth were observed between wild type PA14 and the
439 Δ*oprC* strain (Fig. 6). One reason for the lack of robust OprC-mediated toxicity is that *oprC*
440 might also be repressed by external copper under anaerobic conditions.

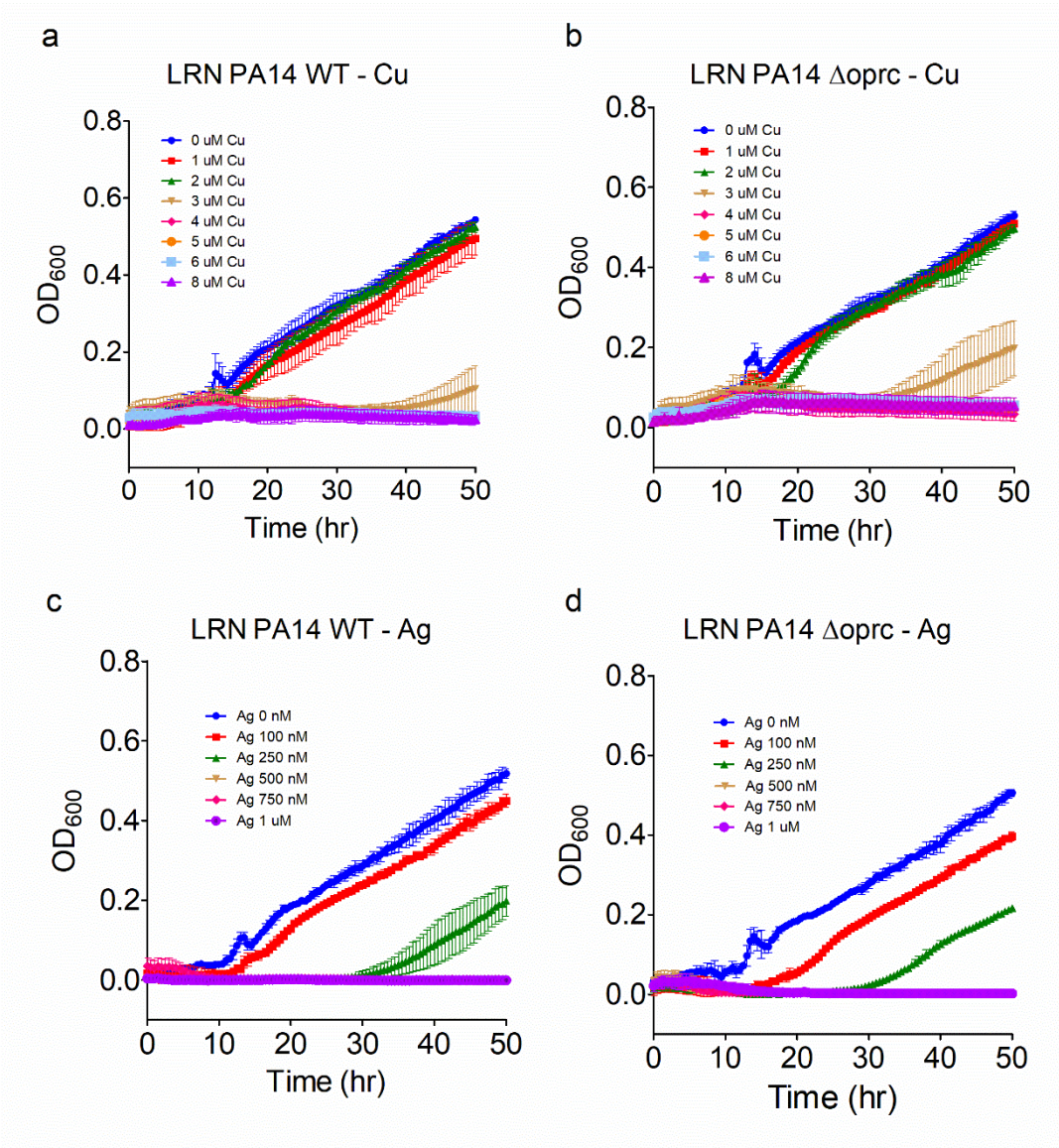


441

442 **Figure 6. Lack of OprC does not alleviate copper toxicity.** *P. aeruginosa* PA14 growth
443 under anaerobic conditions was monitored during copper and silver stress in minimal media.
444 Growth curves of (**a,c**) WT and (**b,d**) Δ*oprC* in LR media supplemented with 100 mM sodium
445 nitrate at increasing concentrations of added Cu(II) (**a,b**) or Ag (**c,d**).
446
447
448 ## Discussion

449 Our combined data define OprC as a specific importer of Cu(I), which is coordinated by a very
450 unusual CxxxM-HxM binding motif in which the cysteine provides a reducing environment.
451 The presence of a methionine binding track in OprC and the involvement of two methionine
452 residues in the principal binding site are consistent with the preference of Cu(I) for S-contain-
453 ing ligands. Methionines also coordinate Cu(I) in other known copper transporters, such as
454 the bacterial CusABC and CopA exporters and the eukaryotic Ctr1 copper importer[16, 18, 38-40].
455 These transporters have been shown to also transport silver, but structures with silver have
456 been determined only for the Cus system[16, 38]. Our structural data strongly suggest that OprC
457 can also import silver. With regards to Cu(II), the picture that emerges from our *in vitro* data
458 with detergent-solubilised protein, is that Cu(II) binds non-specifically to OprC and subse-
459 quently migrates to the principal binding site via an unknown mechanism, where it is reduced
460 to Cu(I). The Cu(II) affinity of 2.6 μM reported by an early study[26] most likely resulted from
461 non-specific binding, since the rich media used[41] to culture *P. aeruginosa* would have gener-
462 ated OprC with 100% copper occupancy in the principal binding site. Whether Cu(II) is a sub-
463 strate for OprC *in vivo* remains an open question. A recent study in *P. aeruginosa* proposed a
464 novel copper uptake mechanism in copper-limited conditions which involves secretion of the
465 copper binding protein azurin by a CueR-regulated Type VI secretion system. The secreted
466 azurin would scavenge Cu(II) from the environment and load it onto OprC via a direct interac-
467 tion, conferring a competitive advantage under copper-limiting conditions[27]. While this model
468 requires further corroboration, our data show that the imported species will be Cu(I).
469
470 The copper site most similar to that in OprC occurs in class I Type I copper proteins like
471 cytochrome c oxidase, pseudoazurin and plastocyanin, electron transfer proteins that
472 coordinate Cu(I) or Cu(II) via a 2Cys+1Met+1His site/2His+1Cys+1Met site. Interestingly,
473 substitution of either of the two OprC binding site methionines with histidine generates M147H
474 and M325H transporters that bind copper with similar efficiency as wild type OprC and, at least
475 in the case of M325H, has a pseudoazurin-like active site with tetrahedral geometry
476 (Supplementary Fig. 8). However, both proteins are still colourless and the spectrum of the
477 Cu-loaded M147H variant is EPR-silent (Supplementary Fig. 4), suggesting the principal
478 binding sites in these variants also comprise a reducing environment and bind Cu(I).
479

480 Given that copper, and in particular the more toxic Cu(I), is a known antimicrobial, the question
481 arises why bacteria have proteins dedicated to Cu(I) acquisition from the environment. Indeed,
482 in contrast to *e.g.* iron that is withheld from a pathogen by the host during infection, host-
483 derived copper is a "nutritional immunity" antimicrobial response. Thus, bacterial virulence is
484 generally attenuated by mutations, particularly in transporters, that cause copper sensitivity[42].
485 No data have yet been reported on the role of OprC in *P. aeruginosa* virulence, but a recent
486 study reported decreased virulence of an *A. baumannii* OprC knockout[43], which is the opposite
487 of what one might expect from the copper nutritional immunity model[42]. In this context, our
488 proteomics data showing that OprC is very abundant in a *P. aeruginosa* mouse infection model
489 are particularly intriguing. Considering the near-irreversible copper binding, we speculate that
490 OprC could also play a role as a copper reservoir on the cell surface. As a TBDT, Cu-loaded
491 OprC depends on TonB for transport, and it is possible that (hypothetical) regulation of the
492 TonB-OprC interaction could "titrate" copper to the periplasmic space as required, when ex-
493 ternal copper is low. Conversely, in the presence of high concentrations of external copper,
494 OprC would be loaded with copper, but this would not lead to import in the absence of an
495 interaction with TonB. This model could provide an alternative explanation for the lack of a
496 robust OprC-dependent growth phenotype in *P. aeruginosa* under copper-replete conditions
497 (Fig. 6). Metallo-proteomes in bacteria are not well characterized, making it challenging to
498 estimate copper requirements[44]. Total cell quantitation suggests a copper concentration of
499 ~40 μM when cells are grown in metal-restricted medium[45]. Assuming a cellular volume of ~1
500 $\mu m^3$ ($10^{-15}$ l), this would correspond to ~25,000 molecules per cell. Thus, a pool of 5,000-
501 10,000 Cu-loaded OprC molecules could provide a substantial part of the total copper content
502 of the cell, most of which will be present as an essential cofactor in enzymes and bound to
503 chaperones and storage proteins. Given this need for copper on the one hand and its toxicity
504 on the other, it is clear that regulation of any copper import protein is crucial, possibly both at
505 the gene and protein level. Unfortunately, and in contrast to the many copper stress genes
506 that, as part of the CopR or CueR regulons, are upregulated under aerobic conditions during
507 copper stress[10, 11, 46-49], nothing is known about how OprC is downregulated during such stress.
508 Intriguingly, *oprC* (*PA3790*) is in an operon with *PA3789*, which encodes for an uncharacter-
509 ised inner membrane protein containing PepSY domains, hinting at a peptidase function. An-
510 other protein strongly downregulated during copper stress is PA5030, which is an MFS trans-
511 porter with a large number of His+Met residues (26 out of 438 residues), suggesting it could
512 mediate copper delivery to the cytoplasm, possibly in concert with OprC and an as yet uniden-
513 tified periplasmic protein[49].
514

515 Bacterial copper import via metallophores is well established. For example, methanotrophic
516 bacteria produce methanobactins that bind copper with micromolar affinity, and are imported
517 by MbnT[22]. In *E. coli,* yersiniabactin (Ybt) binds Cu(II), which is taken up by the FyuA recep-
518 tor[50]. Thus, OprC is the first example of a TBDT that mediates copper import without a metal-
519 lophore. The TBDT with the closest substrate specificity to OprC is the ionic zinc transporter
520 ZnuD from *Neisseria meningitidis*, the structure of which has been solved[51]. Large structural
521 differences between OprC and ZnuD exist for the extracellular loops (overall Cα r.m.s.d. ~5.9
522 Å). ZnuD has several discrete low-affinity binding sites that may guide the metal towards the
523 high-affinity binding site[51]. In OprC, a distinctive "methionine track" provides low-affinity bind-
524 ing sites to guide copper to the high affinity site. Interestingly, while the extracellular loops
525 between OprC and ZnuD are very different and the overall sequence identity is only 28%, the
526 metal binding sites are located at very similar positions and only 2.8 Å apart (Supplementary
527 Fig. 9), suggesting that the transport channel formed via TonB interaction may be similar.
528 Inspection of the ZnuD structure shows that the zinc binding site is excluded from solvent, and
529 we propose that the zinc ion in ZnuD is kinetically trapped, analogous to copper in OprC.
530
531 OprC shares ~60 % identity to NosA from *Pseudomonas stutzeri*, for which no structure is
532 available. Like OprC, NosA is expressed under anaerobic conditions and repressed in the
533 presence of μM concentrations Cu(II)[52-54]. *P. stutzeri* NosA antibodies did not react with *P.*
534 *aeruginosa*[52], but our structure identifies NosA as an OprC ortholog, since the CxxxM-HxM
535 copper binding motif and some of the methionine track residues are conserved
536 (Supplementary Fig. 10). NosA is important during denitrification in *P. stutzeri* JM300 and was
537 proposed to load copper either directly or indirectly to the periplasmic $N_2O$ reductase NosZ[52-
538 54]. However, a more recent report for a different *P. stutzeri* strain found no difference between
539 NosZ activity and copper content for a *nosA* knockout[55]. In addition, OprC/NosA also occurs
540 in a number of non-denitrifying *Proteobacteria* such as *Salmonella enterica, Klebsiella*
541 *pneumoniae* and *Acinetobacter baumannii* (Supplementary Fig. 10), showing that NosZ
542 maturation is not a general function of OprC. The occurrence of OprC in some (*e.g*. *S. enterica*)
543 but not in other (*e.g. E. coli*) Enterobacteria is intriguing, given that the OM of these bacteria
544 is relatively permeable to small molecules due to abundant general porins such as OmpC and
545 OmpF.
546
547 The ability of OprC to take up Cu(I) could be important for biofilms, which are anaerobic to
548 various degrees depending on the location inside the biofilm[56, 57]. Oxygen tension also reduces
549 as lung chronic disease mediated by *P. aeruginosa* progresses, turning airway mucus into an
550 anaerobic environment in cystic fibrosis patients that will favour the availability of Cu(I)[58]. *P.*

551 *aeruginosa* is capable of anaerobic respiration by using nitrate, nitrite or nitrous oxide as
552 terminal electron acceptor[59], and OprC has been shown to be induced under anaerobic
553 conditions[36]. Together, our data suggest that OprC is a novel type of copper transporter for the
554 efficient scavenging of copper under a wide range of physiological conditions, including the
555 anaerobiosis that is a hallmark of disease caused by *P. aeruginosa* in humans.
556

557 **Methods**

558 **Recombinant production of *Pseudomonas aeruginosa* OprC.** The mature version of the
559 gene coding for *oprC* of *P. aeruginosa* PAO1 (UniProt ID; PA3790)[60], starting with His56 as
560 determined by Nakae et al.[26], was synthesized to include a 7 x His tag at the N-terminus
561 (Eurofins, UK), cloned into the pB22 arabinose-inducible expression vector[61] and transformed
562 into chemically competent *Escherichia coli* DH5$\alpha$ cells. After expression and processing by
563 signal peptidase, the N-terminal sequence of this construct is
564 NVRLQHHHHHHHLEAEEHSQHQ-. A second version of this construct was constructed in a
565 pB22 version containing a tobacco etch virus (TEV) site after the His7-tag. Correct sequences
566 were confirmed by DNA sequencing (Eurofins, UK) using both forward and reverse plasmid-
567 specific primers. The $OprC_{AA}$ mutant was produced by changing the key amino acids Cys143
568 and Met147 to alanine residues using the KLD Quickchange site-directed mutagenesis kit
569 (New England Biolabs, UK) and specific primers containing both mutation sites (forward: 5`-
570 tcgcgcggatgcaccaaccagctatattagc-3`; reverse: 5`-ttcggggcggcgccaagcatcatgc-3`). The single
571 mutants C143A, M147A, H323A, M325A, M147H and M325H were made in similar ways.
572

573 OprC recombinant protein production and purification was performed as follows: *E. coli* C43
574 Δ*cyo* was electroporated with expression vector, recovered for 60 minutes in LB (Sigma, UK)
575 at 37 °C, and plated on LB agar (Sigma, UK) containing 100 µg $mL^{-1}$ ampicillin (Melford, UK).
576 Transformants were cultured in LB medium or in LeMasters-Richards (LR) minimal medium
577 with glycerol (2-3 g/l) as carbon source. All media contained 100 µg $mL^{-1}$ ampicillin. For rich
578 media, cells were grown (37 °C, 180rpm) until OD600 ~0.6, when protein expression was
579 induced with 0.1% arabinose for 4-5 h at 30 °C or overnight at 16 °C (150 rpm). For LR media,
580 a small overnight pre-culture in LB was used at 1/100 v/v to inoculate an LR-medium pre-
581 culture early in the morning (typically 1 ml preculture for 100 ml of cells was used), which was
582 grown during the day at 37 °C. After late afternoon inoculation, large-scale cultures (typically
583 6-8 l) were grown overnight at 30 °C until OD 0.4-0.7, followed by induction with 0.1%
584 arabinose at 30 °C for 6-8 hours. Cells were harvested by centrifugation (5,000 rpm, 20
585 minutes, 4 °C), and pellets homogenized in 20 mM Tris (Sigma), 300 mM NaCl (Fisher) pH
586 8.00 (TBS buffer), in the presence of 10 mM ethylene diamine tetraacetic acid (EDTA, Sigma).

587 Cells were broken by one pass through a cell disruptor (Constant Systems 0.75 kW operated
588 at 23 kpsi), centrifuged at 42,000 rpm for 45 minutes at 4 °C (45Ti rotor; Beckman), and the
589 resulting total membrane fraction was homogenized in TBS buffer containing 1.5% Lauryl-
590 dimethylamine oxide (LDAO) (Sigma, UK). Membrane proteins were extracted by stirring (60
591 minutes, 4 °C), centrifuged (42,000 rpm in 45Ti rotor, 30 minutes, 4°C), and the membrane
592 extract was loaded on a Chelating Sepharose Fast Flow bed resin (~10 ml; GE Healthcare,
593 UK) previously activated with 200 mM $NiCl_2$ (Sigma) and equilibrated in TBS containing 0.15 %
594 n-dodecyl-beta-D-maltopyranoside (DDM). After washing with 15 column volumes buffer with
595 30 mM imidazole, protein was eluted with 0.25 M imidazole buffer (Fisher), incubated with 20
596 mM EDTA (30 minutes, 4 °C), and loaded on a Superdex 200 16/600 size exclusion column
597 equilibrated with 10 mM Hepes, 100 mM NaCl, 0.05% DDM, 10 mM EDTA, pH 7.5. Peak
598 fractions were pooled and concentrated using a 50 MWCO Amicon filter (Millipore, UK),
599 analyzed on SDS-PAGE, flash-frozen in liquid nitrogen and stored at -80C. Typical yields of
600 purified wild type and most mutant OprC proteins ranged between 2-5 mg per l media grown
601 at 16 °C. All media and buffer components were made in fresh milli-Q water.
602
603 Protein preparations intended for crystal trials were pooled and buffer-exchanged to 10 mM
604 Hepes 100 mM NaCl, 0.4% tetraethylene glycol mono-octyl ether ($C_8E_4$) (Anatrace, US), pH
605 7.5. $NaNO_3$ was substituted for NaCl for protein preparations intended for crystal trials with
606 silver. Protein preparations to be used for metal analysis after removal of the His-tag
607 underwent a slightly different protocol. The elution fraction from immobilized metal affinity
608 chromatography (IMAC) was buffer-exchanged to 50 mM Tris, 0.5 mM EDTA, 0.2 mM TCEP,
609 100 mM NaCl, 0.05% DDM (Anatrace, US), pH 7.50, and submitted to TEV protease digestion
610 (ratio 1 mg TEV: 10 mg protein, 4 °C, overnight). Samples were submitted to a second IMAC
611 column, where flow-through and wash fractions were combined for the subsequent SEC step
612 in 10 mM HEPES 100 mM NaCl 0.05 % DDM 0.5 mM EDTA pH 7.5. Protein concentration
613 was determined by BCA assay (Thermo Scientific, UK) and by UV/Vis absorbance at 280nm
614 (considering OprC $E_{0.1\%}$ = 1.6 as determined by ProtParam).
615
616 **In vitro metal binding assays and Inductively Coupled Plasma Mass Spectrometry (ICP-**
617 **MS).** OprC samples intended for metal binding assays were exchanged into respective chelex-
618 treated buffers without EDTA and were equilibrated with different equivalents of Cu(II) or Zn,
619 for 30 min at room temperature (n=3). Protein concentrations used were in the range of 10 –
620 20 μM. Samples were loaded on an analytical Superdex 200 Increase 10/300GL (GE
621 Healthcare) column, equilibrated in 10 mM Hepes, 100 mM NaCl, 0.05% DDM, 0.5 mM EDTA
622 pH 7.5. Size exclusion peaks were pooled, concentrated and quantified for protein by UV
623 absorbance at 280 nm. Protein samples were diluted 10-fold in 2.5% $HNO_3$. Analytical metal

624 standards of 0- 500 ppb were prepared by serial dilution from individual metal stocks (VWR,
625 UK) and were matrix-matched to protein samples. Samples and standard curves were
626 analysed by ICP-MS using a Thermo X-series instrument (Thermo Fisher Scientific), and
627 samples were typically screened for the presence of $^{63}Cu$ and $^{65}Zn$.
628
629 **Copper extraction (demetallation) experiments.** $OprC_{WT}$, $OprC_{AA}$ and M147A samples were
630 incubated with 3 equivalents copper for 30 min and then loaded onto a Superdex S-200
631 Increase 10/300GL column equilibrated with 10 mM HEPES 100 mM NaCl 0.05 % DDM 0.5
632 mM EDTA pH 7.5. Peak fractions were pooled, concentrated and quantified by UV absorbance
633 at 280 nm. Samples were exchanged into respective chelex-treated buffer without EDTA. For
634 demetallation experiments, 20 µM of copper-bound proteins were taken in duplicates and
635 incubated with 100-fold excess of the copper chelator bathocuproine disulfonate (BCS)
636 (Sigma) and 100-fold excess of the reducing agent hydroxyl amine ($NH_2OH$) (Sigma) at 60 °C
637 and room temperature. The amount of extracted Cu(I) was quantified by measuring the
638 formation of coloured copper chelate complex, using the complex molar extinction coefficient
639 $\varepsilon_{483nm}$ = 13,300 $M^{-1}$ $cm^{-1}$ [62].
640
641 **Fluorescence spectroscopy**
642 OprC samples in chelex-treated buffers without EDTA were diluted in 10 mM HEPES, 100 mM
643 NaCl, 0.05% DDM (pH 7.5) to a volume of 250 µL and a concentration of 20 µM, and samples
644 were titrated with consecutive additions of Cu(II). Fluorescence emission spectra were rec-
645 orded on a Varian Cary Eclipse spectrophotometer (Agilent). The excitation wavelength was
646 300 nm and emission spectra were recorded between 300 – 500 nm, with excitation slit of 5
647 nm, at a scan rate of 600 nm/min. Data was plotted and analysed for peak changes in the
648 region of 300-400 nm due to Cu(II) binding[63]. Experiments were performed in triplicates under
649 aerobic conditions, and reactions were equilibrated for 5 minutes at room temperature prior to
650 recording each fluorescence spectrum.
651
652 **Protein crystallization, data collection and structure determination.** Sitting-drop
653 crystallization trials were set up using a Mosquito crystallization robot (TTP Labtech) with
654 commercial screens (MemGold1 and MemGold2, Molecular Dimensions) at 20 °C. To obtain
655 the initial structure of Cu-bound OprC, the protein (~12 mg/ml) was incubated with 3 mM $CuCl_2$
656 for 1 hr at room temperature, followed by setting up crystallisation trials. A number of initial hits
657 were obtained and were subsequently optimised by manual hanging drop vapour diffusion
658 using larger drops (typically 1-1.5 ul protein + 1 ul reservoir). Well-diffracting crystals (~3 Å
659 resolution at a home source) were obtained in 0.1 M NaCl/0.15 M $NH_4SO_4$/0.1 M MES pH
660 6.5/18-22% PEG1000. Crystals were cryoprotected with mother liquor lacking $CuCl_2$

661 containing 10% PEG400 for ~5-10 s and flash-frozen in liquid nitrogen. Diffraction data were
662 collected at Diamond Light Source (Didcot, UK) at beamline i02. For the best crystal, belonging
663 to space group $C222_1$, 720 degrees of data were collected at an energy of 8994 eV,
664 corresponding to the K-edge of copper (Supplementary Table 1). Data were auto processed
665 by xia2. The structure was solved via single anomalous dispersion (SAD) via AUTOSOL in
666 Phenix[64]. Two copper sites were found, one for each OprC molecule in the asymmetric unit
667 (Supplementary Fig. 1). The phases were of sufficient quality to allow automated model
668 building via Phenix AUTOBUILD, generating ~60% of the structure and using data to 2.0 Å.
669 The remainder of the structure was built manually, via iterative cycles of refinement in Phenix
670 and model building in COOT[65]. Metal coordination was analysed by the Check-my-metal
671 server[66]. The final refinement statistics are listed in Supplementary Table 1. Subsequently,
672 crystals were also obtained without any copper supplementation of the protein. These were
673 isomorphous to those described above and obtained under identical conditions. Molecular
674 replacement indicated the presence of copper and an identical structure to that obtained above
675 (data not shown). $OprC_{AA}$ crystals (~10 mg/ml protein) were obtained and optimized by
676 hanging drop vapor diffusion as described above, and diffraction-quality crystals were
677 obtained in the same conditions as for Cu-OprC, *i.e*. 0.1 M sodium chloride/0.15 M ammonium
678 sulfate/0.01 M MES sodium pH 6.5/19% (w/v) PEG1000. Interestingly however, the $OprC_{AA}$
679 crystals belong to a different space group ($P22_12_1$), most likely as a result of structural
680 differences between both OprC variants. Diffraction data were collected at Diamond Light
681 Source (Didcot, UK) at beamline I24. Diffraction data were processed in XDS[67]. The structure
682 was solved by molecular replacement (MR) using Phaser, with wildtype OprC as the search
683 model. Model building was done in COOT and refinement in Phenix. As for Cu-OprC, the data
684 collection and refinement statistics are shown in Supplementary Table 1. C143A and H323A
685 proteins (~10 – 12 mg/ml protein) were incubated with 2 mM $CuSO_4$ at room temperature for
686 1 hr, followed by co-crystallisation. Diffracting crystals for both C143A and H323A in the
687 presence of copper were obtained in 0.34 M Ammonium sulfate/0.1 M Sodium citrate pH
688 5.5/12 -16 % w/v PEG 4000 and were cryo-protected using mother liquor lacking $CuSO_4$ and
689 with 25% ethylene glycol for ~10 s and flash-frozen in liquid nitrogen. M147H and M325H
690 crystals were obtained in the same condition as those for wild type OprC. For co-crystallisation
691 with silver, OprC proteins were incubated with 2 mM AgNO3 for 1 hour at room temperature,
692 followed by co-crystallisation. Well-diffracting $OprC_{WT}$ crystals with silver were obtained under
693 the same conditions as in the presence of copper. For the best $OprC_{WT}$ crystal, belonging to
694 space group $C222_1$, 999 degrees of data were collected at an energy of 8000 eV to obtain
695 anomalous signals for Ag. C143A and H323A crystals (~10-12 mg/ml protein) with Ag were
696 obtained from 0.2 M Choline chloride/0.1 M Tris pH 7.5/12-16 % w/v PEG 2000 MME and 0.5
697 M Potassium chloride/0.05 M HEPES pH 6.5/12-16 % v/v PEG 400, respectively. Crystals

698 were cryoprotected for 5-20 s with mother liquor lacking $AgNO_3$ but containing 25% ethylene
699 glycol for C143A and 20 % PEG 400 for H323A. For C143A and M325A crystallised in the
700 presence of copper or silver, datasets of 360 degrees each were collected at energies of 8800
701 and 9175 eV, using different parts of the same crystal (Supplementary Tables 2 and 3).
702
703 **Electron Paramagnetic Resonance Spectroscopy.**
704 Electron Paramagnetic Resonance (EPR) measurements were carried out using a Bruker
705 ELEXSYS-E500 X-band EPR spectrometer operating in continuous wave mode, equipped
706 with an Oxford variable-temperature unit and ESR900 cryostat with Super High-Q resonator.
707 All EPR samples were prepared in quartz capillary tubes (outer diameter; 4.0 mm, inner diam-
708 eter 3.0 mm) and frozen immediately in liquid $N_2$ until further analysis. The experimental setup
709 and conditions were similar to reported earlier[68]. The low temperature EPR spectra were ac-
710 quired using the following conditions: sweep time of 84 s, microwave power of 0.2 mW, time
711 constant of 81 ms, average microwave frequency of 9.44 GHz and modulation amplitude of 5
712 G, T = 20 K. The concentration of $OprC_{WT}$ and mutants varied from 210-260 μM in 10 mM
713 HEPES, 100 mM NaCl, 0.03 % DDM (n-dodecyl-D-maltoside), pH 7.5 and 10 mM HEPES,
714 100 mM $NaNO_3$, 0.4 % C8E4 (tetraethylene glycol monooctyl ether) buffer pH 8, respectively.
715 Analysis and simulations of the cw-EPR spectra were performed using EasySpin toolbox
716 (5.2.28) for the Matlab (R2017a) program package[69, 70].
717
718 **Quantum chemistry calculations.** A truncated version of the crystal structure of OprC (PDB
719 ID 6FOK) consisting of only the copper ion, Cys143, Met147, His323 and Met2325 was used
720 as input for single point energy calculations. The link atoms between these four amino acids
721 and the rest of the protein were capped with hydrogen atoms, giving a total of 70 atoms. The
722 calculations were performed on the system (i) without copper, (ii) with Cu(I) or (iii) with Cu(II).
723 In addition, two possibilities were considered for the state of the cysteine: hydrogenated
724 (reduced) or dehydrogenated (oxidised). The calculations were performed in linear-scaling
725 Density Functional Theory (DFT) with the PBE exchange-correlation functional in ONETEP[71].
726 Norm-conserving pseudopotentials, an energy cutoff of 800 eV and a kernel cutoff of 1000
727 Bohr in open-boundary conditions were used in a cubic box with sides of 30 Å in length.
728 Quantum chemistry calculations produce huge energies because they are the energies of all
729 the electrons (including core electrons) interacting with the nuclei and themselves. However,
730 the total energies are meaningless and what is chemically important are differences between
731 different conformations and different bonding situations, which are typically much smaller as
732 they concern re-arrangements of valence electrons. For this reason, it is crucial to converge
733 the huge total energies very tightly in order to capture the chemically interesting energy
734 differences.

735

736 ***In vivo* metal toxicity assays**

737 For metal toxicity assays in *E. coli,* JW0473-3 (*ΔcopA*)[72] were transformed with plasmids
738 containing $OprC_{WT}$, $OprC_{AA}$ or empty cloning vector (pB22). The copper exporter *copA* mutant
739 was obtained from the Keio collection; Growth assays were set up in flat-bottomed 96-well
740 plates (Thermo Scientific) containing LB-ampicillin supplemented with 0.01% arabinose. Dif-
741 ferent concentrations (0-6mM) of Cu(II) ($CuSO_4$) were tested in order to assess growth phe-
742 notypes under metal excess conditions. Cultures in triplicates were inoculated with 1:100 di-
743 lution of overnight pre-inoculum from isolated colonies. Assays were performed in a plate
744 reader (Tecan Infinite M200), with 37C incubation and regular orbital shaking of 30 seconds
745 at every 5 minutes, for a total of 25 hours. Time points were collected with 30 mins intervals.
746 For metal toxicity assays in *P. aeruginosa*, PA14 WT and PA14 *Δoprc* strains were used and
747 assays were performed in anaerobic conditions. Pre- cultures were grown under anaerobiosis
748 in rich LB or LR minimal media supplemented with 100 mM sodium nitrate. The Cu(II) ($CuSO_4$)
749 range tested varied from 0 – 7 mM in rich media to 0 – 8 μM in LR media. Cultures in triplicates
750 were inoculated with precultures grown in respective media under anaerobic conditions with-
751 out any excess metal added. Plates were set up and sealed inside an anaerobic chamber
752 (Don Whitley Scientific). For silver toxicity, 0 – 1 μM Ag ($AgNO_3$) was used and assays were
753 performed as described for Cu (II) in LR minimal media supplemented with 100 mM $NaNO_3$.
754 Experiments were performed in triplicates for all tested conditions.

755

756 **Animal infection models.**

757 *Intra-tracheal instillation model*: specific pathogen free (SPF) immunocompetent male
758 Sprague-Dawley rats weighing 100 - 120 g or male CD-1 mice weighing 20 - 25 g were infected
759 by depositing an agar bead containing around $10^7$ colony-forming units *Acinetobacter*
760 *baumannii* ATCC 19606 and *Pseudomonas aeruginosa* UCBPP-PA14, deep into the lung via
761 nonsurgical intra-tracheal intubation[73]. In brief, animals were anesthetized with isoflurane (5%)
762 and oxygen (1.5 L/min) utilizing an anesthesia machine. Depth of anesthesia was evaluated
763 by absence of gag reflex; if the reflex was present, the animal was placed back under
764 anesthesia until the reflex disappeared. No animals were utilized until they were fully
765 anesthetized. Animals were infected via intra-bronchial instillation of molten agar suspension
766 (rats- 100 μl) (mice- 20 μl) via intra-tracheal intubation, and then allowed to recover. Animals
767 were returned in their home cages and observed until recovered from anesthesia. At 24 h post
768 infection, animals were sacrificed and lung was homogenized in sterile saline using a lab
769 blender. All procedures are in accordance with protocols approved by the GSK Institutional
770 Animal Care and Use Committee (IACUC), and meet or exceed the standards of the American

771 Association for the Accreditation of Laboratory Animal Care (AAALAC), the United States
772 Department of Health and Human Services and all local and federal animal welfare laws.
773
774 **Sample workup for proteomics**
775 The sample workup protocol was optimized to deplete host material while maintaining *A.*
776 *baumannii* and *P. aeruginosa* viability until lysis. All buffers and equipment were used at 0 to
777 4 °C to minimize proteome changes during sample workup. The sample volume (maximum of
778 1 ml) was estimated and an equal volume of 1% Tergitol in PBS was added followed by
779 vigorous vortexing for 30 s. After centrifugation at 500 x g for 5 min, the supernatant was
780 transferred to a fresh tube, and the pellet was extracted again with 2 ml 0.5% Tergitol in PBS.
781 The supernatant was combined with the first supernatant and centrifuged at 18'000 x g for 5
782 min. The pellet was washed with 2 ml and again centrifuged at 18'000 x g for 5 min. The
783 supernatant was removed, and the pellet was resuspended in 100 µL 5% sodium
784 deoxycholate, 5 mM Tris (2-carboxyethyl) phosphine hydrochloride, 100 mM $NH_4HCO_3$. The
785 sample was incubated at 90°C for 1 min. and then stored at -80 °C. Samples were thawed
786 and sonicated for 2 x 20 s (1 s interval, 100% power). Proteins were alkylated with 10 mM
787 iodoacetamide for 30 min in the dark at room temperature. Samples were diluted with 0.1M
788 ammonium bicarbonate solution to a final concentration of 1% sodium deoxycholate before
789 digestion with trypsin (Promega) at 37°C overnight (protein to trypsin ratio: 50:1). After
790 digestion, the samples were supplemented with TFA to a final concentration of 0.5% and HCl
791 to a final concentration of 50 mM. Precipitated sodium deoxycholate was removed by
792 centrifugation at 4°C and 14'000 rpm for 15 min. Peptides in the supernatant were desalted
793 on C18 reversed phase spin columns according to the manufacturer's instructions (Macrospin,
794 Harvard Apparatus), dried under vacuum, and stored at −80°C until further processing.
795
796 **Parallel reaction monitoring**
797 Heavy proteotypic peptides (JPT Peptide Technologies GmbH) were chemically synthesized
798 for *A. baumannii* and *P. aeruginosa* outer membrane proteins. Peptides were chosen
799 dependent on their highest detection probability and their length ranged between 7 and 20
800 amino acids. Heavy proteotypic peptides were spiked into each sample as reference peptides
801 at a concentration of 20 fmol of heavy reference peptides per 1 µg of total endogenous protein
802 mass. For spectrum library generation, we generated parallel reaction-monitoring (PRM)[74]
803 assays from a mixture containing 500 fmol of each reference peptide. The setup of the µRPLC-
804 MS system was as described previously[75]. Chromatographic separation of peptides was
805 carried out using an EASY nano-LC 1000 system (Thermo Fisher Scientific) equipped with a
806 heated RP-HPLC column (75 µm x 37 cm) packed in-house with 1.9 µm C18 resin (Reprosil-
807 AQ Pur, Dr. Maisch). Peptides were separated using a linear gradient ranging from 97%

808 solvent A (0.15% formic acid, 2% acetonitrile) and 3% solvent B (98% acetonitrile, 2% water,
809 0.15% formic acid) to 30% solvent B over 60 minutes at a flow rate of 200 nl/min. Mass
810 spectrometry analysis was performed on Q-Exactive HF mass spectrometer equipped with a
811 nanoelectrospray ion source (both Thermo Fisher Scientific). Each MS1 scan was followed by
812 high-collision-dissociation (HCD) of the 10 most abundant precursor ions with dynamic
813 exclusion for 20 seconds. Total cycle time was approximately 1 s. For MS1, 3e6 ions were
814 accumulated in the Orbitrap cell over a maximum time of 100 ms and scanned at a resolution
815 of 120,000 FWHM (at 200 m/z). MS2 scans were acquired at a target setting of 1e5 ions,
816 accumulation time of 50 ms and a resolution of 30,000 FWHM (at 200 m/z). Singly charged
817 ions and ions with unassigned charge state were excluded from triggering MS2 events. The
818 normalized collision energy was set to 35%, the mass isolation window was set to 1.1 m/z and
819 one microscan was acquired for each spectrum.
820
821 The acquired raw-files were converted to the mascot generic file (mgf) format using the
822 msconvert tool (part of ProteoWizard, version 3.0.4624 (2013-6-3)). Converted files (mgf
823 format) were searched by MASCOT (Matrix Sciences) against normal and reverse sequences
824 (target decoy strategy) of the UniProt database of *Acinetobacter baumannii* strains ATCC
825 19606 and ATCC 17978, and Pseudomonas aeruginosa UCBPP-PA14, as well as commonly
826 observed contaminants. The precursor ion tolerance was set to 20 ppm and fragment ion
827 tolerance was set to 0.02 Da. Full tryptic specificity was required (cleavage after lysine or
828 arginine residues unless followed by proline), three missed cleavages were allowed,
829 carbamidomethylation of cysteins (+57 Da) was set as fixed modification and arginine (+10
830 Da), lysine (+8 Da) and oxidation of methionine (+16 Da) were set as variable modifications.
831 For quantitative PRM experiments the resolution of the orbitrap was set to 30,000 FWHM (at
832 200 m/z) and the fill time was set to 50 ms to reach a target value of 1e6 ions. Ion isolation
833 window was set to 0.7 Th (isolation width) and the first mass was fixed to 100 Th. Each
834 condition was analyzed in biological triplicates. All raw-files were imported into Spectrodive
835 (Biognosys AG) for protein and peptide quantification.
836
837 **Author contributions**
838 BvdB designed the study. SPB and BvdB expressed, purified, and crystallized proteins. AB
839 collected the diffraction data. SPB and BvdB analysed the diffraction data and refined the
840 structures. SPB performed metal binding and *in vivo* growth experiments. TRY performed ICP-
841 MS analyses. MS performed cw-EPR measurements, simulations and interpreted the data.
842 BB performed quantum energy calculations, supervised by SK. SH performed proteomics ex-
843 periments, supervised by DB. BvdB and SPB wrote the paper.
844

845 **Acknowledgements**

846 We would like to thank Scott Sucoloski, Jennifer Hoover, Josh West (Glaxo Smith Kline) for
847 providing proteomics samples. We would also like to thank Kevin Waldron (Newcastle
848 University) for useful discussions and for carrying out initial ICP-MS analyses. We also thank
849 Deenah Osman and Nigel Robinson (Durham University) for elemental analyses by ICP-MS
850 and helpful discussions, supported by awards BB/L009226/1 and BB/R002118/1 from the
851 Biotechnology and Biological Sciences Research Council, BBSRC, UK. We are indebted to
852 the Diamond Light Source for beam time (proposals mx9948, mx13587 and mx18598) and
853 beamline assistance. MS acknowledges the EPSRC National (UK) EPR Research Facility and
854 Service for use of the EPR spectrometers. MS and BvdB thank Luisa Ciano for the useful
855 discussions at an early stage. The research leading to these results was in part conducted as
856 part of the Translocation consortium (www.translocation.eu) and has received support from
857 the Innovative Medicines Initiatives Joint Undertaking under Grant Agreement No. 115525,
858 resources that are composed of financial contributions from the European Union's seventh
859 framework programme (FP7/2007–2013) and European Federation of Pharmaceutical
860 Industries and Associations companies in-kind contribution. BvdB would also like to
861 acknowledge the Royal Society for salary support.

862

863 **Accession codes**

864 Coordinates and structure factors have been deposited in the Protein Data Bank
865 (http://www.ebi.ac.uk/pdbe/) with accession codes 6FOK ($OprC_{WT}$), 6FOM ($OprC_{AA}$), 6Z8Q
866 ($OprC_{WT}$ Ag 8000 ev), 6Z9I ($OprC_{C143A}$ Ag 8800 eV), 6Z99 ($OprC_{C143A}$ Ag 9175 eV), 6Z8Y
867 ($OprC_{C143A}$ Cu 8800 eV), 6Z8Z ($OprC_{C143A}$ Cu 9175 eV), 6Z8T ($OprC_{H323A}$ Ag 8800 eV), 6Z8U
868 ($OprC_{H323A}$ Ag 9175 eV), 6Z8R ($OprC_{M147H}$), 6Z8S ($OprC_{M325H}$), 6Z9N ($OprC_{H323A}$ Cu 9175 eV),
869 6Z9Y ($OprC_{H323A}$ Cu 8800 eV).

870

871

872 **References**

873 1. Hodgkinson, V. & Petris, M.J. Copper homeostasis at the host-pathogen interface. *The*
874 *Journal of biological chemistry* **287**, 13549-13555 (2012).
875 2. Harrison, J.J., Ceri, H. & Turner, R.J. Multimetal resistance and tolerance in microbial
876 biofilms. *Nature reviews. Microbiology* **5**, 928-938 (2007).
877 3. Lemire, J.A., Harrison, J.J. & Turner, R.J. Antimicrobial activity of metals: mechanisms,
878 molecular targets and applications. *Nature reviews. Microbiology* **11**, 371-384 (2013).
879 4. Braymer, J.J. & Giedroc, D.P. Recent developments in copper and zinc homeostasis
880 in bacterial pathogens. *Current opinion in chemical biology* **19**, 59-66 (2014).

881 5. Robinson, N.J. & Winge, D.R. Copper metallochaperones. *Annual review of*
882 *biochemistry* **79**, 537-562 (2010).
883 6. Hernandez-Montes, G., Arguello, J.M. & Valderrama, B. Evolution and diversity of
884 periplasmic proteins involved in copper homeostasis in gamma proteobacteria. *BMC*
885 *microbiology* **12**, 249 (2012).
886 7. Zimmermann, M. et al. PcoE--a metal sponge expressed to the periplasm of copper
887 resistance *Escherichia coli*. Implication of its function role in copper resistance. *Journal*
888 *of inorganic biochemistry* **115**, 186-197 (2012).
889 8. Vita, N. et al. A four-helix bundle stores copper for methane oxidation. *Nature* **525**,
890 140-143 (2015).
891 9. Arguello, J.M., Raimunda, D. & Padilla-Benavides, T. Mechanisms of copper
892 homeostasis in bacteria. *Frontiers in cellular and infection microbiology* **3**, 73 (2013).
893 10. Zhang, X.X. & Rainey, P.B. Regulation of copper homeostasis in *Pseudomonas*
894 *fluorescens SBW25*. *Environmental microbiology* **10**, 3284-3294 (2008).
895 11. Hu, Y.H., Wang, H.L., Zhang, M. & Sun, L. Molecular analysis of the copper-responsive
896 CopRSCD of a pathogenic *Pseudomonas fluorescens* strain. *Journal of microbiology*
897 **47**, 277-286 (2009).
898 12. Rubino, J.T. & Franz, K.J. Coordination chemistry of copper proteins: how nature
899 handles a toxic cargo for essential function. *Journal of inorganic biochemistry* **107**,
900 129-143 (2012).
901 13. Boal, A.K. & Rosenzweig, A.C. Structural biology of copper trafficking. *Chemical*
902 *reviews* **109**, 4760-4779 (2009).
903 14. Ma, Z., Jacobsen, F.E. & Giedroc, D.P. Coordination chemistry of bacterial metal
904 transport and sensing. *Chemical reviews* **109**, 4644-4681 (2009).
905 15. Gonzalez-Guerrero, M. & Arguello, J.M. Mechanism of Cu+-transporting ATPases:
906 soluble Cu+ chaperones directly transfer Cu+ to transmembrane transport sites.
907 *Proceedings of the National Academy of Sciences of the United States of America* **105**,
908 5992-5997 (2008).
909 16. Su, C.C. et al. Crystal structure of the CusBA heavy-metal efflux complex of
910 *Escherichia coli*. *Nature* **470**, 558-562 (2011).
911 17. Outten, F.W., Huffman, D.L., Hale, J.A. & O'Halloran, T.V. The independent cue and
912 cus systems confer copper tolerance during aerobic and anaerobic growth in
913 *Escherichia coli*. *The Journal of biological chemistry* **276**, 30670-30677 (2001).
914 18. Kulathila, R., Kulathila, R., Indic, M. & van den Berg, B. Crystal structure of *Escherichia*
915 *coli* CusC, the outer membrane component of a heavy metal efflux pump. *PloS one* **6**,
916 e15610 (2011).

917 19. Khalfaoui-Hassani, B. et al. Widespread Distribution and Functional Specificity of the
918 Copper Importer CcoA: Distinct Cu Uptake Routes for Bacterial Cytochrome c
919 Oxidases. *mBio* **9** (2018).
920 20. Ekici, S., Yang, H., Koch, H.G. & Daldal, F. Novel transporter required for biogenesis
921 of cbb3-type cytochrome c oxidase in *Rhodobacter capsulatus*. *mBio* **3** (2012).
922 21. De Feo, C.J., Aller, S.G., Siluvai, G.S., Blackburn, N.J. & Unger, V.M. Three-
923 dimensional structure of the human copper transporter hCTR1. *Proceedings of the*
924 *National Academy of Sciences of the United States of America* **106**, 4237-4242 (2009).
925 22. Dassama, L.M., Kenney, G.E., Ro, S.Y., Zielazinski, E.L. & Rosenzweig, A.C.
926 Methanobactin transport machinery. *Proceedings of the National Academy of*
927 *Sciences of the United States of America* **113**, 13027-13032 (2016).
928 23. Govan, J.R. & Deretic, V. Microbial pathogenesis in cystic fibrosis: mucoid
929 *Pseudomonas aeruginosa* and *Burkholderia cepacia*. *Microbiological reviews* **60**, 539-
930 574 (1996).
931 24. Lyczak, J.B., Cannon, C.L. & Pier, G.B. Establishment of *Pseudomonas aeruginosa*
932 infection: lessons from a versatile opportunist. *Microbes and infection* **2**, 1051-1060
933 (2000).
934 25. Chevalier, S. et al. Structure, function and regulation of *Pseudomonas aeruginosa*
935 porins. *FEMS microbiology reviews* **41**, 698-722 (2017).
936 26. Yoneyama, H. & Nakae, T. Protein C (OprC) of the outer membrane of *Pseudomonas*
937 *aeruginosa* is a copper-regulated channel protein. *Microbiology* **142 ( Pt 8)**, 2137-2144
938 (1996).
939 27. Han, Y. et al. A *Pseudomonas aeruginosa* type VI secretion system regulated by CueR
940 facilitates copper acquisition. *PLoS pathogens* **15**, e1008198 (2019).
941 28. Tsukihara, T. et al. The whole structure of the 13-subunit oxidized cytochrome c
942 oxidase at 2.8 A. *Science* **272**, 1136-1144 (1996).
943 29. Robinson, H. et al. Structural basis of electron transfer modulation in the purple CuA
944 center. *Biochemistry* **38**, 5677-5683 (1999).
945 30. Shibata, N. et al. Novel insight into the copper-ligand geometry in the crystal structure
946 of *Ulva pertusa* plastocyanin at 1.6-A resolution. Structural basis for regulation of the
947 copper site by residue 88. *The Journal of biological chemistry* **274**, 4225-4230 (1999).
948 31. Celia, H. et al. Structural insight into the role of the Ton complex in energy transduction.
949 *Nature* **538**, 60-65 (2016).
950 32. Noinaj, N., Guillier, M., Barnard, T.J. & Buchanan, S.K. TonB-dependent transporters:
951 regulation, structure, and function. *Annual review of microbiology* **64**, 43-60 (2010).
952 33. Frandsen, K.E. et al. The molecular basis of polysaccharide cleavage by lytic
953 polysaccharide monooxygenases. *Nature chemical biology* **12**, 298-303 (2016).

954 34. Hedison, T.M., Heyes, D.J., Shanmugam, M., Iorgu, A.I. & Scrutton, N.S. Solvent-
955 slaved protein motions accompany proton coupled electron transfer reactions
956 catalysed by copper nitrite reductase. *Chemical communications* **55**, 5863-5866
957 (2019).
958 35. Simmons, T.J. et al. Structural and electronic determinants of lytic polysaccharide
959 monooxygenase reactivity on polysaccharide substrates. *Nature communications* **8**,
960 1064 (2017).
961 36. Filiatrault, M.J. et al. Effect of anaerobiosis and nitrate on gene expression in
962 *Pseudomonas aeruginosa*. *Infection and immunity* **73**, 3764-3772 (2005).
963 37. Yamano, Y., Nishikawa, T. & Komatsu, Y. Cloning and nucleotide sequence of
964 anaerobically induced porin protein E1 (OprE) of *Pseudomonas aeruginosa PAO1*.
965 *Molecular microbiology* **8**, 993-1004 (1993).
966 38. Xue, Y. et al. Cu(I) recognition via cation-pi and methionine interactions in CusF.
967 *Nature chemical biology* **4**, 107-109 (2008).
968 39. Ren, F. et al. X-ray structures of the high-affinity copper transporter Ctr1. *Nature*
969 *communications* **10**, 1386 (2019).
970 40. Stoyanov, J.V., Magnani, D. & Solioz, M. Measurement of cytoplasmic copper, silver,
971 and gold with a lux biosensor shows copper and silver, but not gold, efflux by the CopA
972 ATPase of *Escherichia coli*. *FEBS letters* **546**, 391-394 (2003).
973 41. Yoshihara, E. & Nakae, T. Identification of porins in the outer membrane of
974 *Pseudomonas aeruginosa* that form small diffusion pores. *The Journal of biological*
975 *chemistry* **264**, 6297-6301 (1989).
976 42. Ladomersky, E. & Petris, M.J. Copper tolerance and virulence in bacteria. *Metallomics*
977 *: integrated biometal science* **7**, 957-964 (2015).
978 43. Abdollahi, S., Rasooli, I. & Mousavi Gargari, S.L. The role of TonB-dependent copper
979 receptor in virulence of *Acinetobacter baumannii*. *Infection, genetics and evolution :*
980 *journal of molecular epidemiology and evolutionary genetics in infectious diseases* **60**,
981 181-190 (2018).
982 44. Cvetkovic, A. et al. Microbial metalloproteomes are largely uncharacterized. *Nature*
983 **466**, 779-782 (2010).
984 45. Schalk, I.J. & Cunrath, O. An overview of the biological metal uptake pathways in
985 *Pseudomonas aeruginosa*. *Environmental microbiology* **18**, 3227-3246 (2016).
986 46. Thaden, J.T., Lory, S. & Gardner, T.S. Quorum-sensing regulation of a copper toxicity
987 system in *Pseudomonas aeruginosa*. *Journal of bacteriology* **192**, 2557-2568 (2010).
988 47. Teitzel, G.M. et al. Survival and growth in the presence of elevated copper:
989 transcriptional profiling of copper-stressed *Pseudomonas aeruginosa*. *Journal of*
990 *bacteriology* **188**, 7242-7256 (2006).

991 48. Frangipani, E., Slaveykova, V.I., Reimmann, C. & Haas, D. Adaptation of aerobically
992 growing *Pseudomonas aeruginosa* to copper starvation. *Journal of bacteriology* **190**,
993 6706-6717 (2008).
994 49. Quintana, J., Novoa-Aponte, L. & Arguello, J.M. Copper homeostasis networks in the
995 bacterium *Pseudomonas aeruginosa*. *The Journal of biological chemistry* **292**, 15691-
996 15704 (2017).
997 50. Koh, E.I., Robinson, A.E., Bandara, N., Rogers, B.E. & Henderson, J.P. Copper import
998 in *Escherichia coli* by the yersiniabactin metallophore system. *Nature chemical biology*
999 **13**, 1016-1021 (2017).
1000 51. Calmettes, C. et al. The molecular mechanism of Zinc acquisition by the neisserial
1001 outer-membrane transporter ZnuD. *Nature communications* **6**, 7996 (2015).
1002 52. Lee, H.S., Hancock, R.E. & Ingraham, J.L. Properties of a *Pseudomonas stutzeri* outer
1003 membrane channel-forming protein (NosA) required for production of copper-
1004 containing N2O reductase. *Journal of bacteriology* **171**, 2096-2100 (1989).
1005 53. Mokhele, K., Tang, Y.J., Clark, M.A. & Ingraham, J.L. A *Pseudomonas stutzeri* outer
1006 membrane protein inserts copper into N2O reductase. *Journal of bacteriology* **169**,
1007 5721-5726 (1987).
1008 54. Lee, H.S., Abdelal, A.H., Clark, M.A. & Ingraham, J.L. Molecular characterization of
1009 nosA, a *Pseudomonas stutzeri* gene encoding an outer membrane protein required to
1010 make copper-containing N2O reductase. *Journal of bacteriology* **173**, 5406-5413
1011 (1991).
1012 55. Wunsch, P., Herb, M., Wieland, H., Schiek, U.M. & Zumft, W.G. Requirements for
1013 Cu(A) and Cu-S center assembly of nitrous oxide reductase deduced from complete
1014 periplasmic enzyme maturation in the nondenitrifier *Pseudomonas putida*. *Journal of*
1015 *bacteriology* **185**, 887-896 (2003).
1016 56. Flemming, H.C. & Wingender, J. The biofilm matrix. *Nature reviews. Microbiology* **8**,
1017 623-633 (2010).
1018 57. Kragh, K.N. et al. Role of Multicellular Aggregates in Biofilm Formation. *mBio* **7**,
1019 e00237 (2016).
1020 58. Alvarez-Ortega, C. & Harwood, C.S. Responses of *Pseudomonas aeruginosa* to low
1021 oxygen indicate that growth in the cystic fibrosis lung is by aerobic respiration.
1022 *Molecular microbiology* **65**, 153-165 (2007).
1023 59. Hassett, D.J. et al. *Pseudomonas aeruginosa* hypoxic or anaerobic biofilm infections
1024 within cystic fibrosis airways. *Trends in microbiology* **17**, 130-138 (2009).
1025 60. Stover, C.K. et al. Complete genome sequence of *Pseudomonas aeruginosa PAO1*,
1026 an opportunistic pathogen. *Nature* **406**, 959-964 (2000).

1027 61. Guzman, L.M., Belin, D., Carson, M.J. & Beckwith, J. Tight regulation, modulation, and
1028 high-level expression by vectors containing the arabinose PBAD promoter. *Journal of*
1029 *bacteriology* **177**, 4121-4130 (1995).
1030 62. Bagchi, P., Morgan, M.T., Bacsa, J. & Fahrni, C.J. Robust affinity standards for Cu(I)
1031 biochemistry. *Journal of the American Chemical Society* **135**, 18549-18559 (2013).
1032 63. Wijekoon, C.J., Young, T.R., Wedd, A.G. & Xiao, Z. CopC protein from *Pseudomonas*
1033 *fluorescens SBW25* features a conserved novel high-affinity Cu(II) binding site.
1034 *Inorganic chemistry* **54**, 2950-2959 (2015).
1035 64. Adams, P.D. et al. PHENIX: a comprehensive Python-based system for
1036 macromolecular structure solution. *Acta crystallographica. Section D, Biological*
1037 *crystallography* **66**, 213-221 (2010).
1038 65. Emsley, P., Lohkamp, B., Scott, W.G. & Cowtan, K. Features and development of
1039 Coot. *Acta crystallographica. Section D, Biological crystallography* **66**, 486-501 (2010).
1040 66. Zheng, H. et al. Validation of metal-binding sites in macromolecular structures with the
1041 CheckMyMetal web server. *Nature protocols* **9**, 156-170 (2014).
1042 67. Kabsch, W. Xds. *Acta crystallographica. Section D, Biological crystallography* **66**, 125-
1043 132 (2010).
1044 68. Karimov, R.R. & Hartwig, J.F. Transition-Metal-Catalyzed Selective Functionalization
1045 of C(sp(3) )-H Bonds in Natural Products. *Angewandte Chemie* **57**, 4234-4241 (2018).
1046 69. Stoll, S. & Schweiger, A. EasySpin, a comprehensive software package for spectral
1047 simulation and analysis in EPR. *Journal of magnetic resonance* **178**, 42-55 (2006).
1048 70. Stoll, S. & Schweiger, A. in ESR spectroscopy in membrane biophysics, Vol. 27. (eds.
1049 M.A. Hemminga & L.J. Berliner) 299-321 (Springer, Boston, MA, 2007).
1050 71. Prentice, J.C.A. et al. The ONETEP linear-scaling density functional theory program.
1051 *The Journal of chemical physics* **152**, 174111 (2020).
1052 72. Baba, T. et al. Construction of *Escherichia coli K-12* in-frame, single-gene knockout
1053 mutants: the Keio collection. *Molecular systems biology* **2**, 2006 0008 (2006).
1054 73. Hoover, J.L. et al. A Robust Pneumonia Model in Immunocompetent Rodents to
1055 Evaluate Antibacterial Efficacy against *S. pneumoniae, H. influenzae*, *K. pneumoniae*,
1056 *P. aeruginosa* or *A. baumannii. Journal of visualized experiments : JoVE* (2017).
1057 74. Peterson, A.C., Russell, J.D., Bailey, D.J., Westphall, M.S. & Coon, J.J. Parallel
1058 reaction monitoring for high resolution and high mass accuracy quantitative, targeted
1059 proteomics. *Molecular & cellular proteomics : MCP* **11**, 1475-1488 (2012).
1060 75. Ahrne, E. et al. Evaluation and Improvement of Quantification Accuracy in Isobaric
1061 Mass Tag-Based Protein Quantification Experiments. *Journal of proteome research*
1062 **15**, 2537-2547 (2016).
1063